Journal of Radioanalytical and Nuclear Chemistry (2023) 332:4343–4353
https://doi.org/10.1007/s10967-023-09147-1

# U-238, Th-232 series, and Pu-239 + Pu-240 concentration analysis in biological samples of high natural background radiation residents by alpha spectrometry

**Akbar Abbasi[1] · Fatemeh Mirekhtiary[2] · Albandari W. Alrowaily[3] · Hesham M. H. Zakaly[4,5,6]**

Received: 15 March 2023 / Accepted: 9 August 2023 / Published online: 26 September 2023



## Abstract

The purpose of this research was to determine the isotope concentration of the actinide radioelements $^{238}U$, $^{232}Th$ series, and $^{239}Pu$ in biological samples (urine) using the alpha spectroscopy system. The samples were selected from the residence of high natural background radiation (HNBR) area and analyzed using chemical procedure. The separated sample was placed on a membrane filter by the sedimentation method, and it was prepared for counting with the alpha spectrometry system. The average radioactive concentrations found in these samples were as follows: $^{234}U > ^{226}Ra > ^{230}Th > ^{228}Ra > ^{228}Th > ^{224}Ra > ^{232}Th > ^{239}Pu$. The average concentrations of $^{234}U$ and $^{226}Ra$ were much greater than the other radionuclides.


**Keywords** Actinide · Alpha spectroscopy · Biological samples · High natural background radiation (HNBR) area

## Introduction

Uranium and thorium are radioactive substances that can be found in nature, like soil [1–3], sediment [4, 5], water [6–8], and building materials [9–11]. The U and Th isotopes typically are employed in various tracer investigations to assess their influence on the environment and geology. The major three isotopes of natural uranium are $^{238}U$ ($T_{1/2} = 4.468 \times 10^9$ a), $^{235}U$ ($T_{1/2} = 704 \times 10^6$ a), and $^{234}U$ ($T_{1/2} = 2.455 \times 10^5$ a), all of which are alpha (α) emitters [12]. Thorium has three primary isotopes, all of which are alpha emitters: $^{232}Th$ ($T_{1/2} = 1.402 \times 10^{10}$ a), $^{230}Th$ ($T_{1/2} = 7.54 \times 10^4$ a) [13], and $^{228}Th$ ($T_{1/2} = 1.9126$ a) [14].

Higher levels of radioactivity in the environment are connected with increased radiation damage and risk to humans, as evidenced by kidney damage, mutagenicity, bladder and kidney cancer, leukaemia, testis cancer, and lung cancer [15–17]. There are several residential locations on the earth with high natural background radiation (HNBR), such as Guarapari in Brazil, Yangjiang in China, Kerala in India, and Ramsar in Iran. In HNBRs regions like Ramsar, the yearly effective dosage rate can approach 260 mSv $a^{-1}$[2].

Uranium and thorium transfer from one environmental compartment to another in biological systems such as vegetables are dependent on the availability of nuclides in the soil as well as the rate of loss from the interior structure of leaves following translocation. This translocation can add the U and Th to the human food chain. Studies on the HNBR area are necessary because clearer findings about the true risks of radiation should obtained and reasonable levels of radiation protection promoted. Although radiobiological and epidemiological studies in HNBR locations have yet to demonstrate any indication of a substantial increase in health damage compared to that in normal background areas, it is necessary to quantify the U and Th concentrations in

✉ Akbar Abbasi
akbar.abbasi@kyrenia.edu.tr

Hesham M. H. Zakaly
h.m.zakaly@gmail.com

1 Faculty of Engineering, University of Kyrenia, Kyrenia, North Cyprus via Mersin 10, Turkey

2 Faculty of Engineering, Near East University, Nicosia, North Cyprus via Mersin 10, Turkey

3 Department of Physics, College of Science, Princess Nourah Bint Abdulrahman University, P.O. Box 84428, 11671 Riyadh, Saudi Arabia

4 Present Address: Physics Department, Faculty of Science, Al-Azhar University, Assiut Branch, Egypt

5 Computer Engineering Department, Faculty of Engineering and Natural Sciences, Istinye University, 34396, Sarıyer, Istanbul, Turkey

6 Institute of Physics and Technology, Ural Federal University, Ekaterinburg, Russia

biological samples [18], particularly if the linear threshold model is used for dose assessments.

Alpha spectrometry could be used to determine the radioactivity of alpha emitter nuclide in environmental samples. Examples include actinide determination on soil samples and analysis of water samples downstream of uranium mining operations for uranium series radionuclides. The technique is also used for internal dosimetry for workers using the analysis of biological samples such as urine [19].

In recent years, natural radionuclides (U and Th) series determination methods in biological samples have been successfully used in various studies around the world [20–27]. There are different methods for the determination of Th series radionuclides in biological samples, but alpha spectrometry is the most accurate and low minimum detection level (MDL) in comparison with other methods like gamma spectrometry and ICP-mass for short-lived radionuclides. However, in the determination of long-lived $^{234}U$, $^{235}U$, and $^{238}U$, the minimum detection level (MDL) of ICP-MS is better than alpha spectrometry.

This study aimed to determine uranium, thorium, radium, and polonium isotopes in biological samples to provide some basic data on residents living in the HNBR area. For these purposes, the activity concentrations of the most important α -emitters, $^{238}U$ series ($^{234}U$, $^{230}Th$, $^{226}Ra$, and $^{218}Po$) and $^{232}Th$ series ($^{232}Th$, $^{228}Th$, $^{228}Ra$, and $^{224}Ra$) were measured in biological samples collected in Ramsar, Iran.

## Materials and methods

### Study area

Ramsar is located at 36° 53′ N, 50° 41′ E, and has an average elevation of 20 m a.s.l. This city is situated in the Caspian Sea's southern region. Ramesar area has a high natural background radiation (HNBR) area in the Talesh Mahaleh, Ramak, Sadat Mahale, and Chaparsar districts (Fig. 1) [4]. In 2016, the Ramsar area was home to a population of 80,000 residents. However, only approximately 20,000 of them chose to reside in the HNBR zones within the area.

### Samples preparation

The sample preparation includes sampling, dissolution, radiochemical separation, and sample counting [2]. Four urine samples from residency families with ages more than 50 years, each with a volume of 500 ml, were taken from the residence of the HNBR area. After that, 100 ml urine samples were selected to separate possess of each element. $^{232}U$ ($T_{1/2} = 68.9$ a), $^{229}Th$ ($T_{1/2} = 7880$ a), $^{242}Pu$ ($T_{1/2} = 3.73 \times 10^5$ a) and $^{225}Ra$ ($T_{1/2} = 14.9$ d) [13] tracer were added to three blank samples and urine samples as a tracer to measure the separation efficiency. The blank samples were analyzed parallel with urine samples to calculate the difference recovery percentage between blank samples and urine samples. So, there was no significant separation among the alpha-emitting isotopes from the different elements. Also, the concentration of all tracers was corrected for the date of application. In this process, ammonium hydrogen phosphate solution (3 ml 1.3 mol $l^{-1}$) and 1 ml 1.25 mol $l^{-1}$ calcium nitrate (50 mg Ca) were added to the solution. In the next step, by adding concentrated ammonium hydroxide and creating an alkaline environment (pH~9), the actinides in the urine were precipitated as calcium phosphate. The samples were centrifuged at 3000 rpm for ~5 min. The precipitate was centrifuged again at 3000 rpm for about 5 min after being washed once with approximately 20–30 ml of distilled water, and the supernatant was discarded. The obtained sediment, which contained iron phosphate and actinides, was dissolved in concentrated nitric acid ($HNO_3$ 10 ml 6 mol $l^{-1}$) and 10 ml aluminum nitrate ($Al(NO_3)_3$ 2 mol $l^{-1}$) solution. The obtained solution was evaporated. Actinide elements were oxidised by adding 0.5 ml 1.5 mol $l^{-1}$ sodium nitrite ($NaNO_2$) in an acidic environment. In the oxidation process, the actinides of Pu(III) and U(IV) increased to Pu (IV) and U(VI), respectively.

In the next step, the separation of actinides using a chromatography column containing exchange anionic resin (Dowex 8 × 1) was carried out. In this process, Th, Pu, and U actinides were separated individually from anionic resin and collected in a separate container. After pre-conditioning the resins with 10 ml of 8 mol $l^{-1}$ $HNO_3$, the sample is loaded onto the columns at a flow rate of ~1 ml $min^{-1}$ to extract and separate Th, Pu, U and Ra. The columns are rinsed with ~10 ml of 8 mol $l^{-1}$ $HNO_3$ until the effluent turns colorless. The resin in the column was removed, divided into portions, and reloaded into new columns. The resin was blended and then divided equally for individual U, Th Pu and Ra determinations. In addition, the resin fraction was equivalent to about 30 ml of urine. The resin column is rinsed with 10 ml of 12 mol $l^{-1}$ HCl to remove Th, and then the Pu isotopes are eluted into a 50 ml centrifuge tube using 15 ml of 2 mol $l^{-1}$ $HNO_3$. The U isotopes are stripped from the resin column with 1.0 ml of 4 mol $l^{-1}$ HCl followed by 15 ml of 0.01 mol $l^{-1}$ HCl. Consequently, the Ra was eluted in 5 ml of 3 mol $l^{-1}$ $HNO_3$.

However, the preparation of a good quality α-source which should be thin, weightless, uniform, and homogenous on a suitable flat and smooth substrate, is one of the most important prerequisites to obtain a good quality α-spectrum with high resolution, and a small low energy tail contribution [28]. The method used in this research was to create sediment (5 μm) through deposition of sediment by gravity sedimentation. Th and U as Phosphate and Pu as Fluoride sediment were co-precipitated [29, 30]. It was obtained uniformly on the membrane filters. Actinide filters were counted

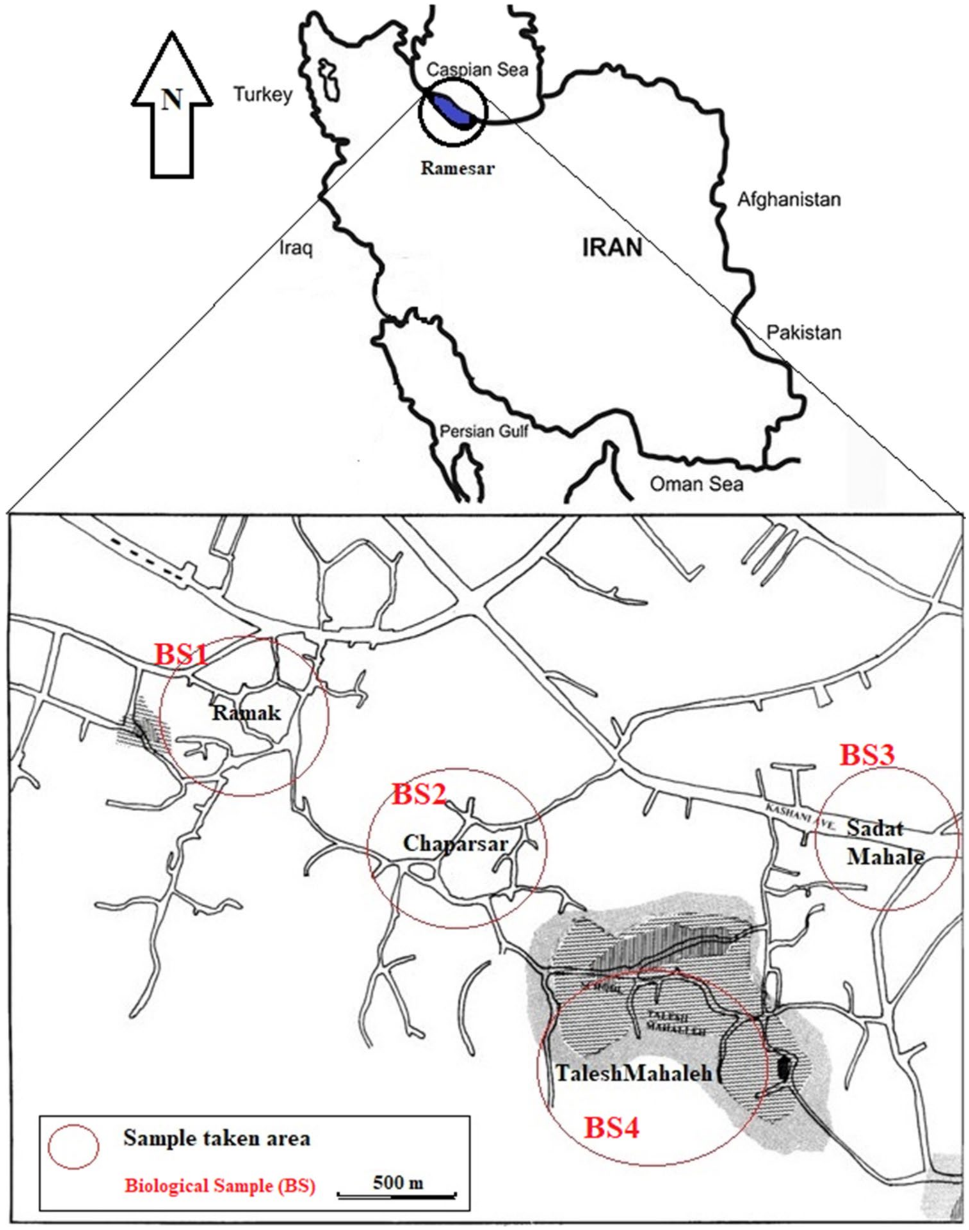


**Fig. 1** The location of biological sampling in high natural background radiation (HNBR) area

by alpha spectrometry for around 16 h; however, depending on the required detection limit, shorter count durations of 1 h can also be achieved for emergency response samples utilizing higher-level tracers [31]. Furthermore, the measurement of $^{228}$Ra concentration was conducted to assess the secular equilibrium between $^{228}$Ra and $^{228}$Ac.

## Samples counting

The Alpha spectrometry system (ALPHAQUATTRO spectroscopy, SILENA, Italy) was applied with a multi-channel analyzer alpha spectroscopy workstation. It incorporates four independent high-quality modular vacuum chambers equipped with high-performance silicon ion implanted charged particle detectors, their associated electronics, a multichannel pulse-height analyzer, and a test pulser [32]. The effective cross-section of the detector was 450 mm$^2$ with an ineffective thickness of 100 µm. The detector has a resolution of approximately 30 keV (FWHM) and a counting efficiency of 20% for a 5 mm source-detector distance calibrated for 3 to 8 MeV energy. Genie 2000 software was applied for data acquisition and count processing. The counting time was 16 h for each sample, and the working voltage of the detector was + 20 V with 1024 channels. In addition, the uncertainty components to calculate the activity concentration combined uncertainty are presented in Table 1. The system was calibrated for energy, resolution, and counting effectiveness using a standard electrodeposited mixed source

**Table 1** Combined standard uncertainties for activity measurements

| Uncertainty components | Combined standard uncertainty of sample BS-1 in percentage unit (%) | | | | | | |
|---|---|---|---|---|---|---|---|
| | $^{234}$U | $^{230}$Th | $^{226}$Ra | $^{232}$Th | $^{228}$Th | $^{228}$Ra | $^{224}$Ra |
| Sample Counts | 2 | 1.3 | 1.9 | 5 | 7 | 5 | 5 |
| Blank Counts | 1 | 1 | 1 | 1 | 1 | 1 | 1 |
| Activity of Tracer | 5 | 5 | 5 | 5 | 5 | 5 | 5 |
| Decay Probability Correction | 1 | 1 | 1 | 1 | 1 | 1 | 1 |
| Sample mass | 2 | 2 | 2 | 2 | 2 | 2 | 2 |
| Time | 0.1 | 0.1 | 0.1 | 0.1 | 0.1 | 0.1 | 0.1 |
| $u_c$ | 11.1 | 10.4 | 12.0 | 14.1 | 16.1 | 14.1 | 14.1 |

of $^{241}$Am, $^{239}$Pu, and $^{244}$Cm to ensure accurate identification and quantification of alpha-emitting radionuclides. In addition, the sample counting sources and the standard calibration source were physically and chemically identical to ensure the accuracy of the results. The uncertainty of the source activities was 4% at the 95% confidence level.

The activity concentration was calculated by applying the following equation:

$$A_{238} = \frac{\frac{C_{238}V_{232}A_{232}I_{232}}{I_{238(C_{232}-C_{228})}} - \frac{C_{238B}V_{232B}A_{232}I_{232}}{I_{238(C_{232B}-C_{228B})}}}{V} \quad (1)$$

where C is counts, V is the tracer volume (l), A is the tracer special activity (Bq/l), I is the decay probability, and V is the sample volume (l). The B index was related to the blank sample.

The minimum detection limit (MDL) was determined using the following equation:

$$MDL\left[\frac{Bq}{g}\right]_{238} = \frac{2.71 + 4.66 \times \sigma_B}{T_B \times \varepsilon \times m_B \times 2.22} \quad (2)$$

where $T_B$ is blank counting time (s), $\varepsilon$ is measurement system efficiency, $m_B$ is mass of blank sample (g), and $\sigma_B$ is:

$$\sigma_{BLK} = \frac{\sqrt{C_{238B}} \times m_{238B} \times A_{232} \times I_{232}}{I_{238} \times (C_{232B} - C_{228B})} \quad (3)$$

where $\sigma_B$ estimated from the standard deviation of multiple blank measurements, and other parameters were explained in the above section.

The $^{228}$Ra radionuclide was measured by HPGe gamma spectrometry system according to the provirus published paper explained method. The gamma lines of 911.2 keV and 969.0 keV emitted from $^{228}$Ac radionuclide were applied to activity calculation (See the method [10]).

### Interferences in the spectrum

The major spectrum interferences for measuring $^{224}$Ra and $^{226}$Ra are predicted to be naturally existing radionuclides in biological samples, such as $^{228}$Th, $^{230}$Th, and $^{234}$U, as well as radium isotope progeny nuclides ($^{226}$Ra, and $^{224}$Ra). Dai et al. [33] report revealed that Th and U distinguish in the urine samples process for $^{226}$Ra, employing chromatographic separation stages using coupled cation/anion exchange columns to ensure efficient Th and U interferences eradication. Because the current process used the same cation/anion exchange separation strategy, the spectrum interferences of $^{230}$Th/$^{234}$U on $^{226}$Ra and $^{228}$Th on $^{224}$Ra were negligible.

Because radium isotopes ($^{226}$Ra and $^{224}$Ra) cannot be chemically separated from each other, possible spectrum interferences between these isotopes and their offspring nuclides must be carefully examined to choose adequate regions of interest (ROI) for calculating radium activity. For the $^{226}$Ra peak at 4.78 MeV and the $^{224}$Ra peak at 5.68 MeV in biological samples, high-energy resolution of the FWHM (full-width at half maximum) ranging from 10 to 30 keV was indicated.

## Results and discussion

### Activity concentration

The activity concentration value of the $^{234}$U, $^{230}$Th, $^{226}$Ra, $^{228}$Th, $^{228}$Ra, $^{224}$Ra and $^{239}$Pu measured in biological (Urine) samples and sample codes area is given in Table 2. The region of interest area technique was applied to measure low-activity concentration radionuclides. The minimum and maximum value of $^{234}$U, $^{230}$Th, $^{226}$Ra, $^{232}$Th, $^{228}$Th, $^{228}$Ra, $^{224}$Ra and $^{239}$Pu were obtained 8011 to 1079 mBq $l^{-1}$, 379 to 681 mBq $l^{-1}$, 4815 to 8830 mBq $l^{-1}$, 4.98 to 7.25 mBq $l^{-1}$, 6.27 to 13.15 mBq $l^{-1}$, 7.18 to 12.17 mBq $l^{-1}$, 4.25 to 8.95 mBq $l^{-1}$, and < MDL, respectively. The order of average concentrations of radionuclides recorded in these samples was as follows; $^{234}$U > $^{226}$Ra > $^{230}$Th > $^{228}$Ra > $^{228}$Th > $^{224}$Ra > $^{232}$Th > $^{239}$Pu. $^{234}$U and $^{226}$Ra were significantly higher than the other measured radionuclides, while in the case of $^{239}$Pu, the average concentrations were lower than MDL (= 5 mBq $l^{-1}$). Table 3 presents the average ratios of $^{224}$Ra/$^{226}$Ra, $^{228}$Ra/$^{226}$Ra, $^{230}$Th/$^{232}$Th, and $^{228}$Th/$^{232}$Th in biological samples were calculated. The higher average value

**Table 2** The activity concentration of $^{238}$U and $^{232}$Th series in biological samples of the study area

| Sample | $^{238}$U Series (mBq l$^{-1}$) | | | 232Th Series (mBq l-1) | | | | $^{239}$Pu (mBq l$^{-1}$) |
|---|---|---|---|---|---|---|---|---|
| | $^{234}$U | $^{230}$Th | $^{226}$Ra | $^{232}$Th | $^{228}$Th | $^{228}$Ra | $^{224}$Ra | |
| BS-1 | 8621 ± 187 | 438 ± 4 | 7620 ± 144 | 5.17 ± 0.01 | 9.28 ± 0.03 | 7.18 ± 0.02 | 8.09 ± 0.01 | < MDL * |
| BS-2 | 8011 ± 174 | 379 ± 4 | 4815 ± 91 | 5.12 ± 0.01 | 7.42 ± 0.02 | 12.01 ± 0.03 | 4.96 ± 0.01 | < MDL * |
| BS-3 | 9172 ± 199 | 491 ± 5 | 6971 ± 131 | 4.98 ± 0.01 | 6.27 ± 0.02 | 12.17 ± 0.03 | 4.25 ± 0.01 | < MDL * |
| BS-4 | 10,079 ± 219 | 681 ± 7 | 8830 ± 166 | 7.25 ± 0.02 | 13.15 ± 0.04 | 10.24 ± 0.02 | 8.95 ± 0.02 | < MDL * |
| Mean | 6720 ± 146 | 497 ± 5 | 7059 ± 133 | 5.63 ± 0.01 | 9.03 ± 0.03 | 10.4 ± 0.02 | 6.56 ± 0.01 | – |
| Min–Max | 8011–10079 | 379–681 | 4815–8830 | 4.98–7.25 | 6.27–13.15 | 7.18–12.17 | 4.25–8.95 | – |

* MDL = 5 mBq l$^{-1}$

was the $^{230}$Th/$^{232}$Th ratio, which shows the difference concentration value of the $^{228}$U series ($^{230}$Th) and $^{232}$Th series. The lower average value was obtained at the $^{224}$Ra/$^{226}$Ra ratio that $^{224}$Ra is from the $^{232}$Th series with low concentration and $^{226}$Ra is from the $^{228}$U series with high concentration in study samples. As per some investigation in the study area, $^{238}$U daughter ($^{226}$Ra) concentration was reported to be higher than the worldwide average [34–36].

Table 3 indicated the ratios of $^{238}$U daughters/$^{238}$U and $^{232}$Th daughters/$^{232}$Th to show disequilibrium in the $^{238}$U and $^{232}$Th decay chains. As demonstrated in Table 3, the average equilibrium ratio in the $^{232}$Th series and its progeny was found to be greater than one, whereas the equilibrium ratio in the $^{238}$U series and its progeny was less than one. Those results show that the radionuclide retention and excretion biokinetic results from this study are consistent with the ICRP models [37].

The comparison of the measured activity concentration of all radionuclides showed that the activity concentration of $^{234}$U was higher than other radionuclides. The activity concentration of $^{226}$Ra in spring water was reported to be more than 146,000 mBq L$^{-1}$ in the study area [34]. Therefore, $^{226}$Ra with a high concentration of water can enter the human organs through the food chain.

The activity concentration percentage of $^{238}$U series ($^{234}$U, $^{228}$Th, $^{226}$Ra, and $^{224}$Ra) and $^{232}$Th series ($^{232}$Th, $^{228}$Th, $^{228}$Ra, and $^{224}$Ra) radionuclides in biological samples are presented in Fig. 2-a and Fig. 2b, respectively. As shown in Fig. 2a, more than 95% of activity concentration was related to two elements of $^{234}$U and $^{226}$Ra. Whiles in the $^{232}$Th series, the activity concentration percentage was distributed between 15 to 40% in measured radionuclides (Fig. 2b).

## Statistical interpretation

To estimate, the correlations between the activity concentration of $^{226}$Ra–$^{234}$U, $^{226}$Ra–$^{228}$Ra, and $^{232}$Th–$^{224}$Ra, $^{232}$Th–$^{228}$Th, $^{232}$Th–$^{230}$Th in biological samples, Spearman correlation analysis was applied. This kind of investigation is beneficial for determining whether there are any probable links between observed activity concentrations of all primordial radionuclides. According to Spearman's correlation, a strong positive correlation was observed between $^{234}$U and $^{226}$Ra (r = 0.977). The correlation coefficient between two sets of variables was determined, and the significance level was decided depending on the sample size. A highly significant correlation was with $p < 0.023$, whereas, $p > 0.05$ was not a significant correlation. For the highly significant correlations regression line (with $R^2 = 95.47\%$) and the prediction were plotted in Fig. 3a. While there is no positive correlation between them and $^{228}$Ra and $^{226}$Ra. This correlation is negative (r = -0.501) with a $p$-value of more than 0.05 ($p = 0.488$) and an R-square value of $R^2 = 26.18\%$. The regression and prediction were plotted in Fig. 3b.

Figure 4a shows the relation between $^{232}$Th concentrations and $^{224}$Ra as a linear model plot. As can be seen from

**Table 3** The activity concentration ratio of $^{224}$Ra/$^{226}$Ra, $^{228}$Ra/$^{226}$Ra, $^{230}$Th/$^{232}$Th, $^{228}$Th/$^{232}$Th; and $^{230}$Th/$^{234}$U, $^{226}$Ra/$^{234}$U, $^{228}$Ra/$^{232}$Th and $^{224}$Ra/$^{232}$Th in biological samples of study area

| Sample | Radionuclide ratios from different chains | | | Radionuclide ratios from the same chain | | | | |
|---|---|---|---|---|---|---|---|---|
| | $^{224}$Ra/$^{226}$Ra | $^{228}$Ra/$^{226}$Ra | $^{230}$Th/$^{232}$Th | $^{228}$Th/$^{232}$Th | $^{230}$Th/$^{234}$U | $^{226}$Ra/$^{234}$U | $^{228}$Ra/$^{232}$Th | $^{224}$Ra/$^{232}$Th |
| BS-1 | 0.00106 ± 0.00002 | 0.00123 ± 0.00005 | 84.72 ± 0.06 | 1.79 ± 0.07 | 0.0508 ± 0.0005 | 0.8839 ± 0.0006 | 1.39 ± 0.07 | 1.56 ± 0.08 |
| BS-2 | 0.00103 ± 0.00002 | 0.00151 ± 0.00007 | 74.02 ± 0.05 | 1.45 ± 0.04 | 0.0473 ± 0.0004 | 0.6010 ± 0.0005 | 2.34 ± 0.12 | 0.97 ± 0.05 |
| BS-3 | 0.00061 ± 0.00001 | 0.00093 ± 0.00003 | 98.59 ± 0.08 | 1.26 ± 0.03 | 0.0535 ± 0.0005 | 0.7600 ± 0.0006 | 2.44 ± 0.16 | 0.85 ± 0.04 |
| BS-4 | 0.00101 ± 0.00002 | 0.00154 ± 0.00004 | 93.93 ± 0.06 | 1.81 ± 0.08 | 0.0676 ± 0.0007 | 0.8761 ± 0.0006 | 1.41 ± 0.08 | 1.23 ± 0.06 |
| Mean | 0.00093 ± 0.00002 | 0.00135 ± 0.00005 | 87.82 ± 0.06 | 1.58 ± 0.06 | 0.0548 ± 0.0005 | 0.7803 ± 0.0005 | 1.89 ± 0.09 | 1.15 ± 0.05 |

**Fig. 2** The activity concentration percentage of **a** $^{238}U$ series ($^{234}U$, $^{230}Th$, $^{226}Ra$ and $^{218}Po$) and **b** $^{232}Th$ series ($^{232}Th$, $^{228}Th$, $^{228}Ra$ and $^{224}Ra$) in biological samples

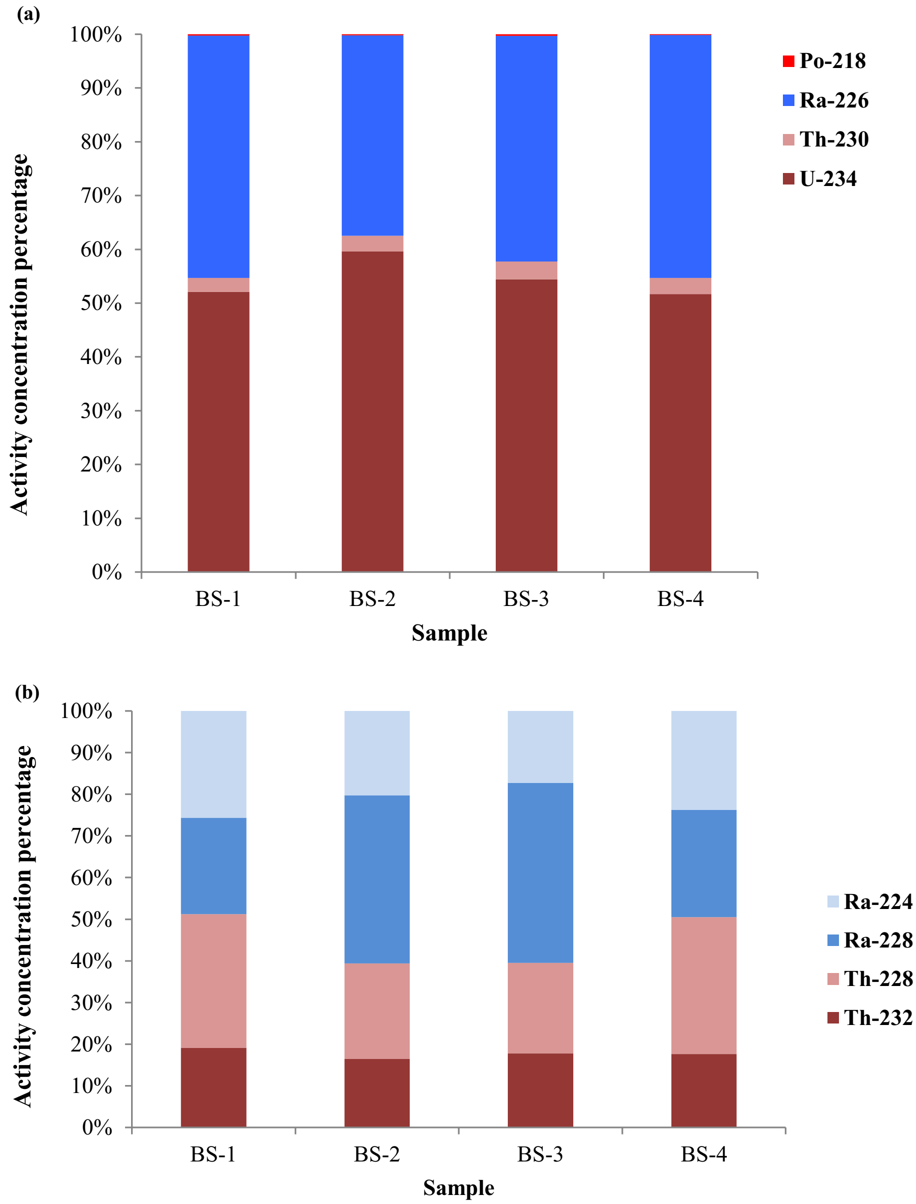


the Figure, our results show a direct significant relationship between $^{224}Ra$ levels and $^{232}Th$ ($r = 0.963$, p-value $< 0.037$). The R-square value (92.77%) and predication plot are shown a strong correlation between $^{232}Th$ and $^{224}Ra$ concentration. These results are also not surprising since both radionuclides are part of the same decay series.

The narrow width of the prediction plot shows this relation (see Fig. 4b). This correlation was expected due to the sameness of the radionuclides in the series and the absence of gaseous elements between these two radionuclides in the decay chain.

The correlation between $^{232}$ and $^{230}Th$ concentrations fitted in the liner model and presented in Fig. 4-c. As can be seen, the measured concentration indicates that there is no significant relation between $^{232}$ and $^{230}Th$. A *p*-value of more than 0.05 (0.395) and $r = 65\%$ indicate this weak relation. The correlation between radionuclides is presented in Table 4.

Within the $^{238}U$ and $^{232}Th$ decay chains, there exist certain parent and daughter relationships that exhibit relatively weak correlations. Furthermore, there are some surprisingly strong and unexpected correlations between isotopes across the $^{238}U$ and $^{232}Th$ chains. These discrepant relationships are generally explained by invoking the rationale of chemical effects within the human body and by local geochemical fractionation processes. The alternative rationale for the presence or lack of correlations among the radionuclides within and across the $^{238}U$ and $^{232}Th$ decay chains is due to the limited statistical strength of the study with only $n = 4$ test donors. With these interpretations, we conclude that the

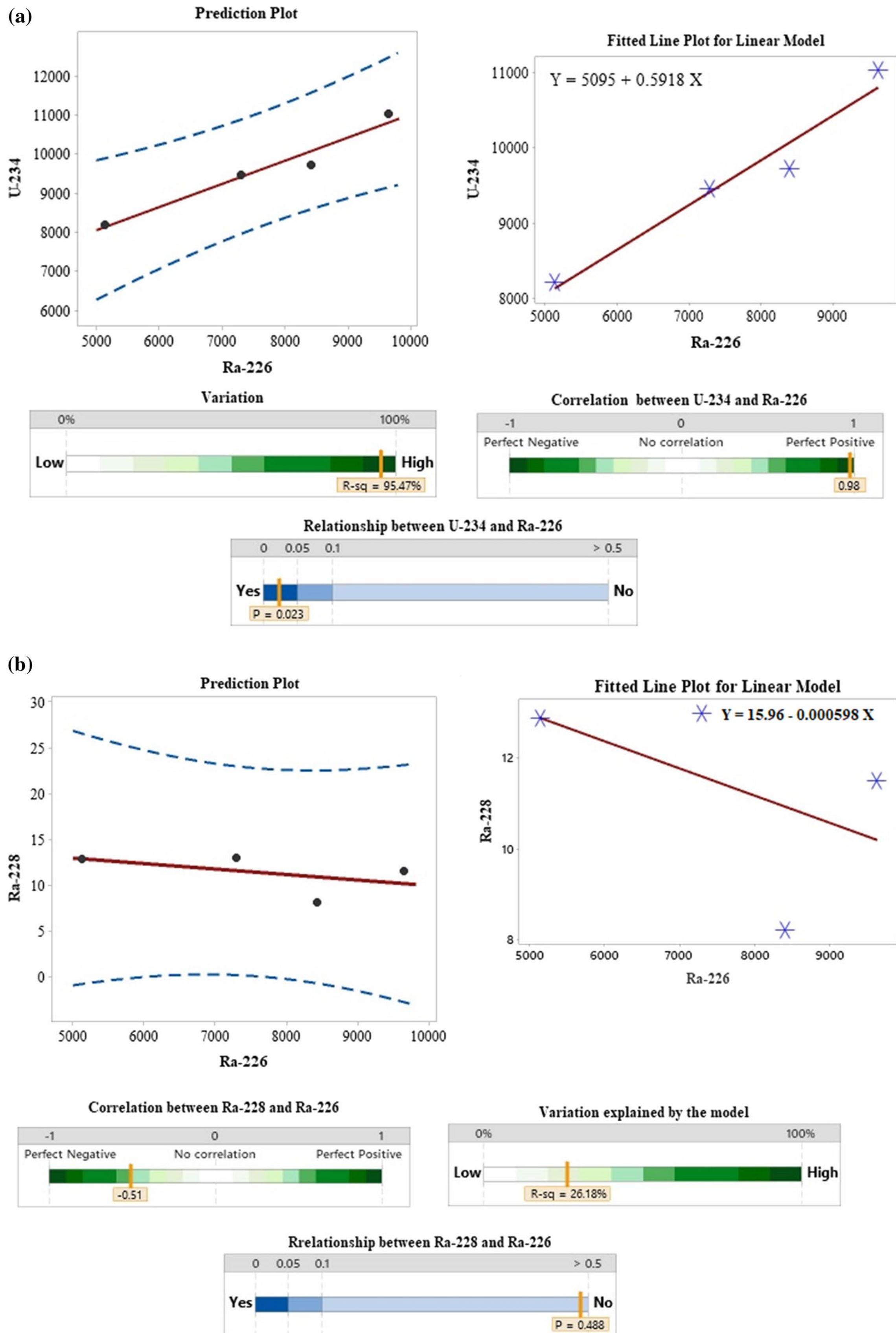


**Fig. 3** The Spearman's correlation and prediction plot of **a** $^{234}$U and $^{226}$Ra, **b** $^{228}$Ra and $^{226}$Ra

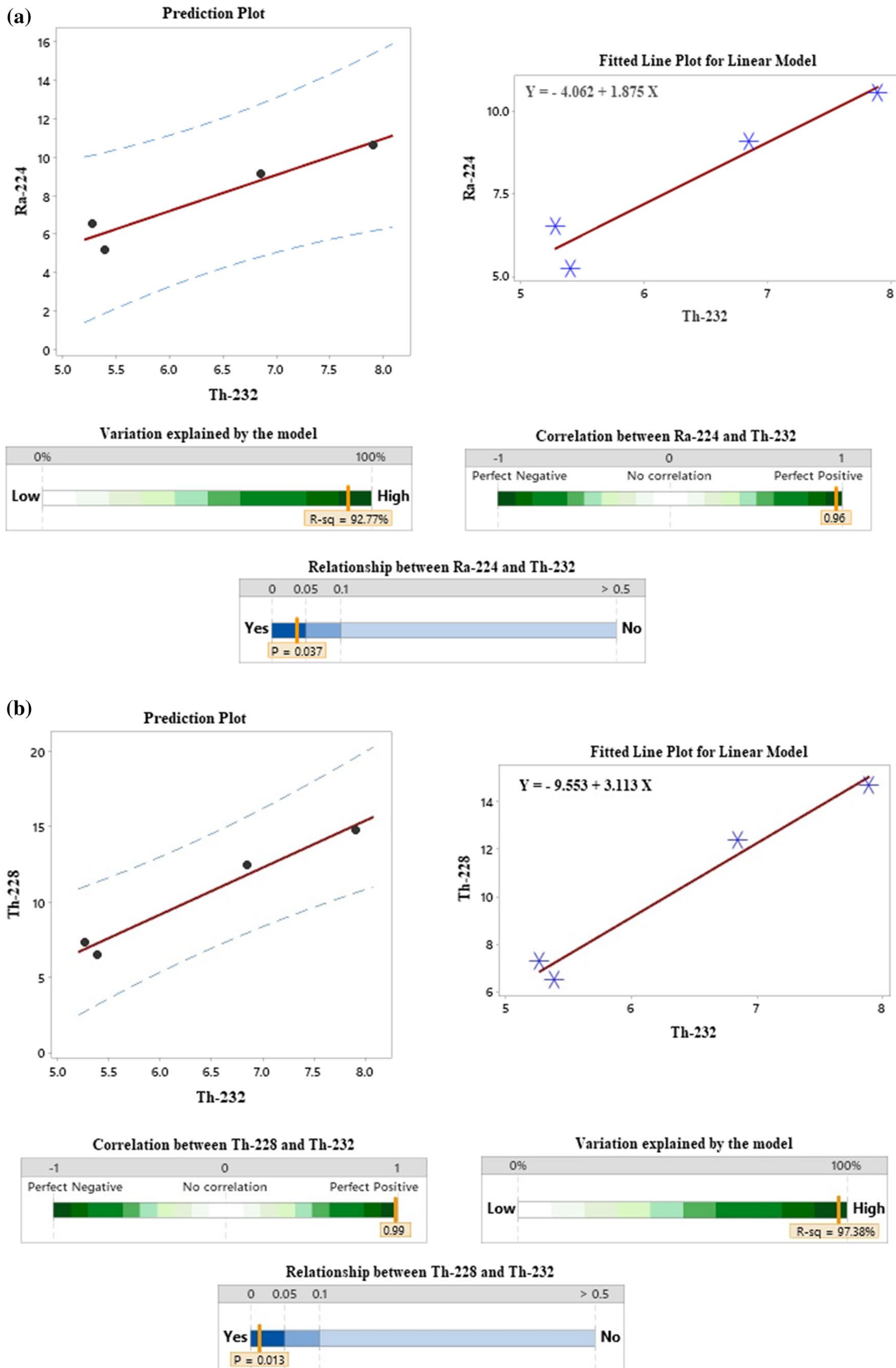


**Fig. 4** The Spearman's correlation and prediction plot of **a** $^{224}$Ra and $^{232}$Th, **b** $^{228}$Th and $^{232}$Th, **c** $^{230}$Th and $^{232}$Th

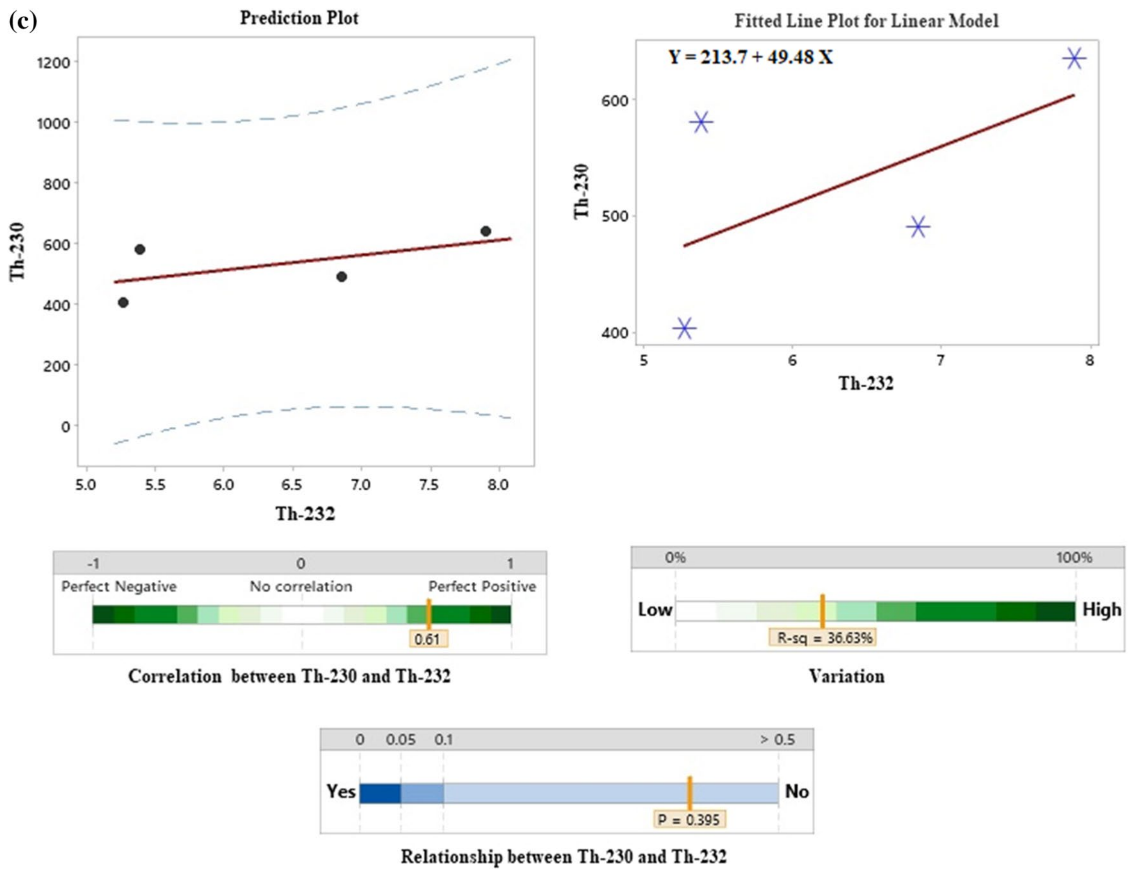


**Fig. 4** (continued)

**Table 4** The concentration correlation between measured radionuclides

| | $^{234}$U | $^{230}$Th | $^{226}$Ra | $^{232}$Th | $^{228}$Th | $^{228}$Ra | $^{224}$Ra |
|---|---|---|---|---|---|---|---|
| $^{234}$U | 1.000 | | | | | | |
| $^{230}$Th | 0.891 | 1.000 | | | | | |
| $^{226}$Ra | 0.977 | 0.821 | 1.000 | | | | |
| $^{232}$Th | 0.897 | 0.395 | 0.904 | 1.000 | | | |
| $^{228}$Th | 0.818 | 0.471 | 0.845 | 0.987 | 1.000 | | |
| $^{228}$Ra | −0.330 | 0.039 | −0.501 | −0.545 | −0.632 | 1.000 | |
| $^{224}$Ra | 0.746 | 0.373 | 0.766 | 0.963 | 0.991 | -0.607 | 1.000 |

importance of the first scenario (biokenetik) was more than that of the second scenario (limited statistical strength). The strong correlations found in Figs. 4 and 5 indicate, that the results in Table 3 indicate a significant correlation. In addition, the cluster similarity diagram of $^{234}$U, $^{228}$Th, $^{226}$Ra, $^{224}$Ra, $^{232}$Th, $^{228}$Th, $^{228}$Ra, $^{224}$Ra and $^{239}$Pu are presented in Fig. 5. The high similarity in concentration trend was observed in two groups of radionuclides. Those radionuclide groups are indicated in Fig. 5.

In addition, Fig. 5 and Table 4 results indicate that $^{228}$Ra was more correlated with the $^{238}$U decay chain than the $^{232}$Th chain. Because of chemical reactions within the human body and local geochemical fractionation, this phenomenon can be explained.

## Conclusion

In this study, $^{238}$U series ($^{234}$U, $^{230}$Th, and $^{226}$Ra), $^{232}$Th series ($^{232}$Th, $^{228}$Th, $^{228}$Ra, and $^{224}$Ra), and $^{239}$Pu of HNBR (Ramsar) were analyzed in biological samples (urine) by radiochemical separation followed by alpha-spectrometry spectra. The significant concentration of $^{234}$U and $^{226}$Ra

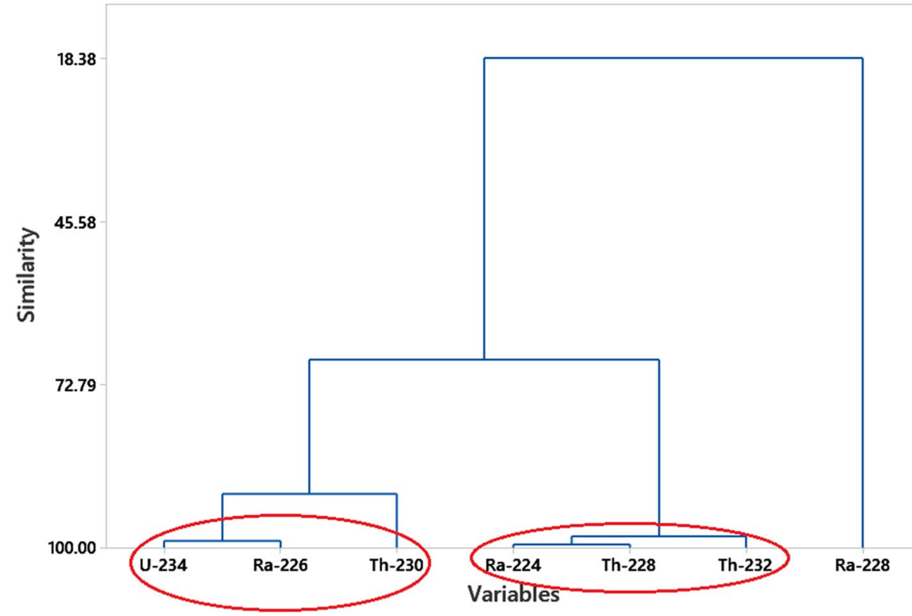


**Fig. 5** The cluster similarity diagram of measured radionuclides in the biological sample

was measured in biological samples (urine), while $^{239}$Pu concentration was not determined and the concentration level was less than MDL. Also, the activity concentration ratio of $^{224}$Ra/$^{226}$Ra, $^{228}$Ra/$^{226}$Ra, $^{230}$Th/$^{232}$Th and $^{228}$Th/$^{232}$Th was calculated. The significant ratio value was obtained for $^{230}$Th/$^{232}$Th radionuclides. Overall, the analysis of activity concentration ratios of radionuclides in decay series provides valuable information about the processes controlling their distribution in the environment, their mobility, and the timescales involved in their radioactive decay. The statistical analysis was carried out to determine the correlation between radioelements. The correlation results indicate that the radionuclide retention and excretion biokinetic ICRP model is the dominant process of being in the same group in a radioactive decay series. According to the findings of this results living in areas with high natural radiation background (HNRB) can pose unique health and safety considerations for residents. Residents who are living in these areas are suggested to undergo periodic health checks.

**Acknowledgements** The authors express their gratitude to Princess Nourah bint Abdulrahman University Researchers Supporting Project (Grant No. PNURSP2023R378), Princess Nourah bint Abdulrahman University, Riyadh, Saudi Arabia, and Guilan University.

**Author contributions** AA: experiments, data processing, original draft, and manuscript preparation. FM: lab analysis, manuscript revision. AWA: methodology, software, HMHZ: methodology, software, writing—original draft preparation, writing—review and editing.

**Funding** The authors express their gratitude to Princess Nourah bint Abdulrahman University Researchers Supporting Project (Grant No. PNURSP2023R378), Princess Nourah bint Abdulrahman University, Riyadh, Saudi Arabia.

## Declarations

**Conflict of interest** The authors declare that they have no known competing financial interests or personal relationships that could have appeared to influence the work reported in this paper.

## References

1. Tawfic AF, Zakaly HMH, Awad HA et al (2021) Natural radioactivity levels and radiological implications in the high natural radiation area of Wadi El Reddah. Egypt. J Radioanal Nucl Chem 327:1–10
2. Abbasi A, Mirekhtiary SF (2020) Radiological impacts in the high-level natural radiation exposure area residents in the Ramsar, Iran. Eur Phys J Plus. https://doi.org/10.1140/epjp/s13360-020-00306-x
3. Abbasi A, Kurnaz A, Turhan Ş, Mirekhtiary F (2020) Radiation hazards and natural radioactivity levels in surface soil samples from dwelling areas of North Cyprus. J Radioanal Nucl Chem 324:1–8
4. Zakaly HM, Uosif MA, Madkour H et al (2019) Assessment of natural radionuclides and heavy metal concentrations in marine sediments in view of tourism activities in Hurghada city, northern Red Sea, Egypt. J Phys Sci 30:21–47. https://doi.org/10.21315/jps2019.30.3.3
5. Abbasi A, Mirekhtiary F (2020) Heavy metals and natural radioactivity concentration in sediments of the Mediterranean Sea coast. Mar Pollut Bull. https://doi.org/10.1016/j.marpolbul.2020.111041
6. Abbasi A (2018) A review of the analytical methodology to determine Radium-226 and Radium-228 in drinking waters. Radiochim Acta. https://doi.org/10.1515/ract-2018-2967
7. Abbasi A, Mirekhtiary F (2019) Lifetime risk assessment of Radium-226 in drinking water samples. Int J Radiat Res. https://doi.org/10.18869/acadpub.ijrr.17.1.163
8. Abbasi A, Mirekhtiary F (2017) Gross alpha and beta exposure assessment due to intake of drinking water in Guilan, Iran. J Radioanal Nucl Chem. https://doi.org/10.1007/s10967-017-5493-6

9. Asgharizadeh F, Abbasi A, Hochaghani O, Gooya ES (2011) Natural radioactivity in granite stones used as building materials in Iran. Radiat Prot Dosimetry 149:321–326
10. Abbasi A (2013) Calculation of gamma radiation dose rate and radon concentration due to granites used as building materials in Iran. Radiat Prot Dosimetry. https://doi.org/10.1093/rpd/nct003
11. Awad HA, Zakaly HMH, Nastavkin AV et al (2021) Radioactive mineralizations on granitic rocks and silica veins on shear zone of El-Missikat area, Central Eastern Desert. Egypt. Appl Radiat Isot 168:109493. https://doi.org/10.1016/j.apradiso.2020.109493
12. (2023) http://www.lnhb.fr/nuclear-data/nuclear-data-table/. In: Lab. Natl. Henri Becquerel
13. (2023) https://www.nndc.bnl.gov/ensdf/EnsdfDispatcherServlet
14. Wysocka I, Vassileva E (2018) Determination of ultra-trace level of 232Th in seawater by ICP-SFMS after matrix separation and preconcentration. Anal Chim Acta 1000:144–154
15. Storm HH, Jørgensen HO, Kejs AMT, Engholm G (2006) Depleted uranium and cancer in Danish Balkan veterans deployed 1992–2001. Eur J Cancer 42:2355–2358
16. Kurttio P, Salonen L, Ilus T et al (2006) Well water radioactivity and risk of cancers of the urinary organs. Environ Res 102:333–338
17. Jia G, Torri G, Magro L (2009) Concentrations of 238U, 234U, 235U, 232Th, 230Th, 228Th, 226Ra, 228Ra, 224Ra, 210Po, 210Pb and 212Pb in drinking water in Italy: reconciling safety standards based on measurements of gross α and β. J Environ Radioact 100:941–949
18. Sohrabi M (1998) The state-of-the-art on worldwide studies in some environments with elevated naturally occurring radioactive materials (NORM). Appl Radiat Isot 49:169–188
19. Vajda N, Pöllänen R, Martin P, Kim C-K (2020) Alpha spectrometry. Handbook of radioactivity analysis. Elsevier, Amsterdam, pp 493–573
20. Thakur P, Ward AL, González-Delgado AM (2021) Optimal methods for preparation, separation, and determination of radium isotopes in environmental and biological samples. J Environ Radioact 228:106522
21. Venus M, Puntarić D, Gvozdić V et al (2019) Determinations of uranium concentrations in soil, water, vegetables and biological samples from inhabitants of war affected areas in eastern Croatia (ICP-MS method). J Environ Radioact 203:147–153
22. Gray PJ, Zhang L, Xu H et al (2012) Determination of 236U/238U and 235U/238U isotope ratios in human urine by inductively coupled plasma mass spectrometry. Microchem J 105:94–100
23. Al-Mashhadani AH, Saleh DS, Razzaq DF (2020) Measurement the uranium, radon and radium concentrations in urine samples for diabetics in Najaf city. In: IOP Conference Series: Materials Science and Engineering. IOP Publishing, p 72108
24. Zoriy MV, Kayser M, Izmer A et al (2005) Determination of uranium isotopic ratios in biological samples using laser ablation inductively coupled plasma double focusing sector field mass spectrometry with cooled ablation chamber. Int J Mass Spectrom 242:297–302
25. Salih NF, Jafri ZM, Aswood MS (2016) Measurement of radon concentration in blood and urine samples collected from female cancer patients using RAD7. J Radiat Res Appl Sci 9:332–336
26. Xiao G, Button J (2022) Rapid determination of 235U/238U in urine using Q-ICP-MS by a simple dilute-and-shoot approach. J Radioanal Nucl Chem 332:1–7
27. Zakaly HMH, Uosif MAM, Issa SAM et al (2021) An extended assessment of natural radioactivity in the sediments of the mid-region of the Egyptian Red Sea coast. Mar Pollut Bull 171:112658
28. Vukanac I, Šešlak B, Kandić A et al (2022) A comparison of alpha-particle and gamma-ray spectrometry methods for determination of 235U, 238U and 226Ra activity concentration in samples of coal, slag and fly-ash. Radiat Phys Chem 193:109933
29. Dai X, Kramer-Tremblay S (2010) Rapid bioassay methods for actinides in urine. In: International Conference on Nuclear Engineering. pp 719–721
30. Reis A, Temba E, Kastner G, Monteiro R (2011) Combined procedure using radiochemical separation of plutonium, americium and uranium radionuclides for alpha-spectrometry. J Radioanal Nucl Chem 287:567–572
31. Maxwell S (2008) Rapid analysis of emergency urine and water samples. J Radioanal Nucl Chem 275:497–502
32. SILENA (1998) SILENA INTERNATIONAL S.p.A
33. Dai X, Kramer-Tremblay S, Li C (2012) Rapid determination of 226Ra in urine samples. Radiat Prot Dosimetry 151:30–35
34. Sohrabi M, Beitollahi MM, Hafezi S et al (1999) Effective dose to the public from 226Ra in drinking water supplies of Iran. Health Phys 77:150–153
35. AminiBirami F, Moore F, Kardan MR et al (2021) Source of 226 Ra in Ramsar spring water, Iran: implication of water–rock interaction and stable isotopes. Environ Earth Sci 80:1–17
36. Awad HAM, Zakaly HMH, Nastavkin AV, El-Taher A (2020) Radioactive content and radiological implication in granitic rocks by geochemical data and radiophysical factors, Central Eastern Desert, Egypt. Int J Environ Anal Chem. https://doi.org/10.1080/03067319.2020.1830987
37. Committee on Internal Exposure International Commission on Radiological Protection, (ICRP) (1988) Limits for intakes of radionuclides by workers, vol. 19. Pergamon Press, pp 1–17